HEFAT2014
10th International Conference on Heat Transfer, Fluid Mechanics and Thermodynamics
14 – 26 July 2014
Orlando, Florida

CFD modeling of chemical looping combustion in fuel reactor with gaseous fuel

Luming Chen[a], Xiaogang Yang[a,*], Xia Li[b], Guang Li[a]

[a]International Doctoral Innovation Centre (IDIC)
The University of Nottingham Ningbo
University Park, Ningbo 315100, P.R. China
[b]Faculty of Engineering, The University of Nottingham
University Park, Nottingham NG7 2RD, UK

Email: Luming.Chen@nottingham.edu.cn
Xiaogang.Yang@nottingham.edu.cn
Xia.Li@nottingham.ac.uk
Guang.Li@nottingham.edu.cn

ABSTRACT

Chemical looping combustion (CLC) as a potential CO_2 capture technology has been considered as a promising and likely alternative to traditional combustion technology to mitigate the CO_2 emission due to its prosecution of CO_2 sequestration at a very low cost. In CLC, solid oxygen carriers are introduced to transfer the oxygen necessary for the combustion from air through the initial oxidation in air reactor and subsequent reduction in fuel reactor. The CLC unit utilized in this study is composed of two interconnected fluidized bed including a circulating fluidized bed as the air reactor and a bubbling fluidized bed as the fuel reactor. While a number of studies on the hydrodynamic behaviour of the CLC process in fuel reactor have been documented in the open literature, there have been limited studies on the correlation between the bubble formation and the local volume fraction. The hydrodynamic behaviours and reactive characteristics of oxygen carriers are still not fully understood although a variety of experiments and simulations have been performed. This paper aims to investigate the CLC process in a fuel reactor using the CFD modelling, coupled with the heterogeneous reactions and investigating the hydrodynamics and reaction kinetics of the CLC process in the fuel reactor. A parameter correlating the occurrence of bubble and dynamic parameters is proposed. The parameter can be acted as an indicator of time-dependent bubble evolution with a potential to be adopted in the CLC for controlling the bubbling phenomena since the occurrence of the bubbles at specific positions is highly correlated with the local large eddies embedded in the flow. The static bed height variations in the fuel reactor system affecting the flow behaviour and kinetics of the CLC process are also discussed. The results obtained from the CFD simulations indicate clearly that the CFD model developed in the current study reasonably forecasts the hydrodynamic behaviour and important phenomena observed in the fuel reactor.

INTRODUCTION

Chemical looping combustion (CLC) has been considered as a promising alternative to traditional combustion technology to mitigate the CO_2 emission due to the potential of CO_2 sequestration at a very low cost. According to the estimation, a coal-fired power plant needs to consume around 20% of the total electricity generated to separate and compress the produced CO_2 in the combustion while CO_2 separation process is responsible for consuming almost three-fourths of the whole energy in the process (1, 2). In addition, coal combustion causes enormous environmental problems. Thus, the application of the CLC may partially resolve the problem. In a CLC, solid oxygen carriers, usually highly-reactive metal particles, are introduced to transfer the oxygen necessary for the combustion from air through the initial oxidation in air reactor and to subsequently realize the reduction in fuel reactor. Until very recently, most of the adopted CLC reactors are based on fluidised bed technology due to its distinct benefits of uniformed particle mixing and temperature gradients together with the continuous operation mode in the fluidized bed reactor. Meanwhile, the bubbling fluidized bed is usually acted as the fuel reactor due to the benefits of controllable handling of particles, high heat flow and relatively high rate of gas-solid reaction leading to the large gas-solid contact area (3). So far, the most common type of CLC reactor is composed of a conventional circulating fluidized bed operated as the air reactor and a bubbling fluidized bed acted as the fuel reactor, as shown in Figure [2]. It should be noticed that the use of the packed (4), moving (5, 6) or circulating fluidized bed (7) to operate as the fuel reactor has also received the attentions and

have been investigated to assess their capabilities. A schematic of the typical CLC unit is shown in Figure 1 (8).

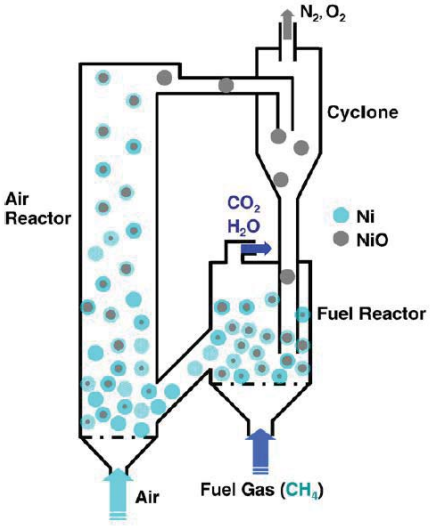

Figure 1. Schematic of two interconnected CLC reactors (8).

NOMENCLATURE

C	[Mol/m^3]	Bulk concentration of gaseous reactant
C_{D0}	[-]	Standard drag coefficient of Gidaspow drag model
d_s	[m]	Diameter of particle
D_{gs}	[m^2/s^2]	The interaction between the fluctuating gas velocity and the fluctuating particle velocity
$\vec{g}$	[m/s^2]	Acceleration due to gravity
g_0	[-]	Radial distribution function
h_{sg}	[W/m^{2}K]	Heat transfer coefficient between gas and solid phase
H	[J/kg]	Enthalpy
I	[-]	Unit tensor
$\bar{\bar{I}}$	[-]	Unit tensor
$\overrightarrow{J_{i,j}}$	[kg/m^2]	Diffusive mass flux
k	[W/mK]	Thermal conductivity
Nu	[-]	Nusselt number
Pr	[-]	Prandtl number
p	[N/m^2]	Gas pressure
P_s	[N/m^2]	Solid pressure
Q_{gs}	[W/m^2]	Heat transfer from the gas phase to solid phase
Q_{sg}	[W/m^2]	Heat transfer from the solid phase to gas phase
Re_p	[-]	Renolds number of particles
R_{he}	[kmol/m^{3}s]	Heterogeneous reaction rate
S_{pq}	[kg/m^{3}s]	Mass transfer from the p_{th} to q_{th} phase
$\vec{u}$	[m/s]	Velocity
U_{sl}	[m/s]	Slip velocity
X	[-]	Conversion
$Y_{i,j}$	[-]	Mass fraction of species j in phase i

Special characters

α_{space}	[-]	Space correlation parameter
α_{time}	[-]	Time correlation parameter
ε	[-]	Volume fraction
ρ	[kg/m^3]	Density
μ	[N.s/m^2]	Viscosity
μ_s	[kg/ms]	Solid shear viscosity
$\mu_{s,col}$	[kg/ms]	Solid collision viscosity
$\mu_{s,kin}$	[kg/ms]	Solid motion viscosity
$\mu_{s,fr}$	[kg/ms]	Solid frictional viscosity
β_{sg}	[kg/m^{3}s]	Drag coefficient
λ_g	[N s/m^2]	Gas bulk viscosity
λ_s	[N s/m^2]	Solid bulk viscosity
$\boldsymbol{\tau_s}$	[N/m^2]	Stress tensor of solid phase
$\bar{\bar{\tau}}_i$	[N/m^2]	Stress tensor of i_{th} phase
Θ_s	[m^2/s^2]	Granular temperature
Φ	[kg/ms^2]	Exchange of fluctuation energy
γ	[kg/ms^3]	Dissipation rate

Subscripts

g	Gas phase
s	Solid phase

This paper aims to investigate the CLC process in a fuel reactor using the CFD modelling, coupled with the heterogeneous reactions and investigating the hydrodynamics and reaction kinetics of the CLC process in the fuel reactor.

Development of oxygen carriers, fundamental design of the CLC reactor and the CLC system analysis has been documented (9-11). Experimental studies on the CLC systems operated with different types of fuels in the range from 300W to 140kW have been performed (12-16), with the findings being summarised in the literature (10, 11). Kolbitsch et al. (2010) assessed the capability of Ni-based oxygen carriers within a 120kW dual circulating fluidized bed reactor system (12) and the authors found that the oxygen transport capacity in both syngas and methane conversion processes using such system presents excellent reactivity. It was identified that besides high reactivity and oxygen transport capacity, no tendency to agglomeration is presented by Ni-based oxygen carriers expect for NiO/TiO_2 (17). The studies (18, 19) have reported that high fuel conversion up to 98-99% without gas leakage was observed within the long-term run of the 10kW CLC unit using Ni-based oxygen carriers. When using the other oxygen carriers, Garcia-Labian et al. (2009) revealed that the sulfur compound like H_2S in fuel gas deactivates the reactivity of Ni-based particles and reduces the combustion efficiency because of the formation of nickel sulfide (20).

Compared with the experimental approach for investigation of the CLC, Computational fluid dynamics (CFD) approach can be easily adopted to investigate the interactions between hydrodynamics and chemical kinetics of the CLC process with a compromise between the level of accuracy and the computational cost. In CFD modeling of the CLC process, both gas and solid phases are treated as continuous and interpenetrating phases in the time and phase averaged Navier-Stokes equations. Wang et al. (2011) and Seo et al. (2011) investigated, respectively, the hydrodynamic behaviours of the full CLC loop using the simplified two-dimensional cold-flow model (21) (22) CFD modelling of the flow behaviours and reactive characteristics of different oxygen carriers in the fuel reactors was also reported (8, 23, 24) and the predictions were in reasonable agreement with the experimental results.

Kruggel-Emden et al. (2010) developed a 2-D interconnected multiphase CFD model using a buffer which can maintain a stable and sufficient solid flow rate into the fuel reactor. In their CFD modelling, the air reactor and the fuel reactor are simulated separately, involving an exchange of solid flow by using the time-dependent sinks and specifying the suitable boundary conditions (25). Wang et al. (2014) studied the CLC process in the DCFB reactors using CFD code – a revised K-FIX program with implementation of the reaction kinetics (26) into the simulation. A reasonable agreement between the simulation and experimental results was claimed. Although these studies have provided to some extent the physical insights into the fluid dynamics involved in the CLC process, there are many fundamental problems remained to be resolved, e.g. how the bubble formation correlates with large vortices in the fuel reactor. In the present study, an attempt to develop a CFD model coupled with heterogeneous reaction for analysing the CLC process in the fuel reactor will be made, aiming at partially answering the above question. Methane is chosen as fuel gas while NiO as coated on $NiMgAl_2O_4$ particles will be used as the oxygen carrier, similar to the work reported in (27).

The paper will be organised in such a way. Section 2 will present the mathematical modelling adopted in the current study while section 3 will present the simulation results and discussion, focusing on bubble formation and distributions of reactants and products in the fuel reactor and characterisation of the bubbling using the correlation between the velocity fluctuations and local volume fraction. Section 4 will present the conclusions derived from the study.

MATHEMATICAL MODELLING

This study assumes the solid particles in the fuel reactor to be spherical and uniform in size and density. The commercial CFD software ANSYS FLUENT was employed to carry out the simulation. Eulerian-Eulerian two-fluid model was used to describe the continuity, exchange of momentum, heat and mass transfer between gas-solid flows while the kinetic theory of granular flow was adopted to model the solid phase. The governing equations are described below:

The continuity equations

For gas phase

$$\frac{\partial}{\partial t}(\varepsilon_g \rho_g) + \nabla \cdot (\varepsilon_g \rho_g \overrightarrow{u_g}) = \mathrm{S}_{gs} \tag{1}$$

For Solid phase

$$\frac{\partial}{\partial t}(\varepsilon_S \rho_S) + \nabla \cdot (\varepsilon_S \rho_S \overrightarrow{u_S}) = \mathrm{S}_{sg} \tag{2}$$

where $S_{gs} = -S_{sg}$ accounts for the mass transfer between gas and solid phases due to heterogeneous reactions; ε, ρ, u are the volume fraction, density and instantaneous velocity respectively. The sum of the volume fraction of each phase must be equal to one.

Momentum Balance Equations

The momentum equations for both phases are given respectively by equation (3) and (4):

$$\frac{\partial}{\partial t}(\varepsilon_g \rho_g \overrightarrow{u_g}) + \nabla \cdot (\varepsilon_g \rho_g \overrightarrow{u_g}\overrightarrow{u_g}) = -\varepsilon_g \nabla p + \nabla \overline{\overline{\tau_g}} + \varepsilon_g \rho_g \vec{g} - \beta(\overrightarrow{u_g} - \overrightarrow{u_S}) + S_{gs}\overrightarrow{u_g} \tag{3}$$

$$\frac{\partial}{\partial t}(\varepsilon_S \rho_s \overrightarrow{u_s}) + \nabla \cdot (\varepsilon_s \rho_s \overrightarrow{u_s}\overrightarrow{u_s}) = -\varepsilon_s \nabla p + \nabla \overline{\overline{\tau_s}} + -\nabla P_S + \varepsilon_g \rho_g \vec{g} + \beta(\overrightarrow{u_g} - \overrightarrow{u_S}) + S_{sg}\overrightarrow{u_s} \tag{4}$$

where, β is the interphase drag coefficient, $\vec{g}$ is the gravity, p is the gas pressure and P_s is the solid pressure. Constitutive closure models are adopted to provide the constitutive equations which are essential for the closure of the governing equations. The gas and solid tensor are given by Equations (5) and (6)

$$\overline{\overline{\tau_g}} = \mu_g\{[\nabla \mathrm{u}_g + (\nabla \mathrm{u}_g)^T] - \frac{2}{3}(\nabla \cdot \mathrm{u}_g)\overline{\overline{I}}\} \tag{5}$$

$$\overline{\overline{\tau_S}} = \mu_S\{[\nabla \mathrm{u}_S + (\nabla \mathrm{u}_S)^T] - \frac{2}{3}(\nabla \cdot \mathrm{u}_S)\overline{\overline{I}}\} + \lambda_S \nabla \cdot u_S \overline{\overline{I}} \tag{6}$$

where, μ is the viscosity, λ_s represents the solid bulk viscosity, $\bar{\bar{I}}$ is the unit tensor.

Energy equations

The energy balance equations of gas and solid phases are given by:

$$\frac{\partial(\varepsilon_g \rho_g H_g)}{\partial t} + \nabla \cdot (\varepsilon_g \rho_g \overrightarrow{u_g} H_g) = \nabla \cdot (k_g \nabla T_g) + Q_{gs} + S_{sg} H_g \tag{7}$$

$$\frac{\partial(\varepsilon_S \rho_S H_S)}{\partial t} + \nabla \cdot (\varepsilon_S \rho_S \overrightarrow{u_S} H_S) = \nabla \cdot (k_S \nabla T_S) + Q_{sg} + S_{gs} H_S \tag{8}$$

Where, H and k represent the enthalpy, thermal conductivity, respectively. $Q_{gs} = -Q_{sg}$, accounting for the inter-phase heat transfer. The heat exchange Q_{sg} can be calculated based on Equation (9)

$$Q_{sg} = h_{sg}(T_g - T_S) \tag{9}$$

where h_{sg} is the heat transfer coefficient between gas and solid phase and is given by Equation(10)

$$h_{sg} = \frac{6 k_g \varepsilon_S \varepsilon_g Nu}{d_S^2} \tag{10}$$

The Nusselt number Nu in aforementioned equation can be calculated based on the empirical relationships as suggested in (28):

$$Nu = (7 - 10\varepsilon_g + 5\varepsilon_g^2)(1 + 0.7\,\mathrm{Re}^{0.2}\mathrm{Pr}^{1/3}) + (1.33 - 2.4\varepsilon_g + 1.2\varepsilon_g^2)\,\mathrm{Re}^{0.7}\mathrm{Pr}^{1/3} \quad (11)$$

With the given Prandtl number Pr, the particle Renolds number Re_p and the particle diameter d_p.

Species transport equations:

The conservation equations of species *j*, which are used to describe the chemical reactions in the fuel reactor are given by

$$\frac{\partial(\varepsilon_i \rho_i Y_{i,j})}{\partial t} + \nabla \cdot (\varepsilon_i \rho_i \overline{u_i} Y_{i,j}) = -\nabla \cdot (\varepsilon_i \overrightarrow{J_{i,j}}) + \mathrm{R}_{he} \quad (12)$$

where $Y_{i,j}$ denotes the mass fraction of species *j* in phase *i* , $\overrightarrow{J_{i,j}}$ the diffusive mass flux and R_{he} the heterogeneous reaction rate.

Drag Model

Several drag models for gas-solid bubbling fluidized bed (the Wen-Yu, Syamlal-O'Brien and Gidaspow drag models) have been proposed to illustrate the inter-phase momentum exchange between phases (29). However, Gidaspow drag model was employed in the current study since it has been widely accepted and utilised in the simulation of fluidized beds at commercial scale (30).

$$\beta_{sg} = 150\frac{\varepsilon_s^2}{\varepsilon_g}\frac{\mu_g}{d_p^2} + 1.75\varepsilon_s\frac{\rho_g}{d_p}\left|\overrightarrow{u_g} - \overrightarrow{u_s}\right|, \quad \text{for } \varepsilon_g \le 0.8 \quad (13)$$

$$\beta_{sg} = 0.75\left|\overrightarrow{u_g} - \overrightarrow{u_s}\right|\varepsilon_g \rho_g \mathrm{C}_{D0}\,\varepsilon_g^{-2.65}\frac{\left(1-\varepsilon_g\right)}{d_p}, \quad \text{for } \varepsilon_g \ge 0.8 \quad (14)$$

Where, C_{D0} is the standard drag coefficient.

$$C_{D0} = 0.44, \ \text{for } \mathrm{Re}_p > 1000; \qquad C_{D0} = \frac{24}{\mathrm{Re}_p}(1 + 0.15\,\mathrm{Re}_p^{0.687}), \ \mathrm{Re}_p \le 1000; \quad (15)$$

With the particle Reynolds number $Re_p = \frac{\rho_g d_p (u_g - u_p)\varepsilon_g}{\mu_g}$.

Kinetic Theory of Granular Flow (KTGF)

The kinetic theory of granular flow (KTGF) is basically an extension of the classical kinetic gas theory and it has been utilised to interpret the random granular motion of particle collision in fluidized bed. In the KTGF, the rheology of fluidized particles is dominated by the fluctuating motion and local concentration of solids. The KTGF expresses the particle collision using two parameters, the solid phase stresses and viscosities, which are represented in turn as a function of granular flow temperature. This study adopts the equation as described in (31, 32).

$$\frac{3}{2}\left[\frac{\partial}{\partial t}\left(\varepsilon_S \rho_S \Theta\right) + \nabla \cdot \left(\varepsilon_S \rho_S \Theta\right) \mathrm{u}_S\right] = \left(-\nabla \mathrm{p}_S \mathrm{I} + \tau_S\right) : \nabla \mathrm{u}_S + \nabla \cdot \left(\mathrm{k}_S \nabla \Theta\right) - \gamma_S + \Phi_S + \mathrm{D}_{gs} \quad (16)$$

In Equation (16), the two terms on the left hand side account for the accumulation and convection of kinetic fluctuation energy separately. The first term on the right hand side depicts the production of kinetic fluctuation energy due to irreversible deformation of the solid phase velocity field, while the conductive transport of kinetic fluctuation energy is described by the second term. The third term is used to model the dissipation of the fluctuation energy resulted from the inelastic inter-particle interactions. The fourth term indicates the exchange of the fluctuation energy owing to the interphase momentum transport. The interaction between the fluctuating gas velocity and the fluctuating particle velocity represented by the last term is usually neglected due to the complete suppression of gas phase turbulence in bubbling gas-solid fluidized beds (32).

The diffusion of fluctuation energy k_s can be defined based on the work reported in (33):

$$k_s = k_s^{dense} + k_s^{thin} \quad (17)$$

$$k_s^{dense} = \frac{15\rho_s d_s \varepsilon_s \sqrt{\Theta_s \pi}}{4(41-33\eta)}\left[1 + \left(\frac{12}{5}\eta(4\eta-3) + \frac{16}{15\pi}(41-33\eta)\right)\eta\varepsilon_s \mathrm{g}_0\right] \quad (18)$$

$$k_s^{thin} = \frac{25\rho_s d_s \sqrt{\Theta_s \pi}}{16 g_0 \eta(41-33\eta)}\left[1 + \frac{12}{5}\eta^2(4\eta-3)\varepsilon_s \mathrm{g}_0\right] \quad (19)$$

$$\eta = 0.5(1+e) \quad (20)$$

With the given coefficient of restitution *e*. The estimation of the dissipation of the fluctuation energy due to particle collision following (33) is given by

$$\gamma_s = 12(1-e^2)\varepsilon_s^2 \rho_s \sqrt{\frac{\Theta_s^3}{\pi d_p^2}} \quad (21)$$

The exchange of the fluctuation energy owing to the interphase momentum transport can be defined by (31):

$$\Phi_s = -3\beta\Theta_s \quad (22)$$

The solid pressure P_s can be defined (33):

$$P_S = [1 + 2(1+e)\varepsilon_S g_0]\varepsilon_S \rho_S \Theta_S \quad (23)$$

where g_0 is the radial distribution function as proposed by Ding and Gidaspow (31):

$$g_0 = \frac{3}{5}[1 - (\frac{\varepsilon_S}{\varepsilon_{S,\max}})^{1/3}]^{-1} \quad (24)$$

The solid bulk viscosity λ_s can be evaluated based on Lun [*]:

$$\lambda_S = \frac{4}{3}\varepsilon_S \rho_S d_p g_0 (1+e)\sqrt{\frac{\Theta_S}{\pi}} \quad (25)$$

The solid shear viscosity can be assumed to be a linear superposition of the viscosities individually contributed by particle collisions, particle motion and frictional effects, which is given by

$$\mu_S = \mu_{S,col} + \mu_{S,kin} + \mu_{S,fr} \quad (26)$$

$$\mu_{s,col} = \frac{4}{5}\varepsilon_s \rho_s g_0 d_p (1+e)\sqrt{\frac{\Theta}{\pi}} \quad (27)$$

$$\mu_{S,kin} = \frac{10 d_S \rho_S \sqrt{\Theta_S \pi}}{96\varepsilon_S (1+e) g_0}[1 + \frac{5}{4}\varepsilon_S g_0 (1+e)]^2 \quad (28)$$

$$\mu_{S,fr} = \frac{P_S \sin\zeta}{2\sqrt{I_{2D}}} \quad (29)$$

with the second invariant of the deviatoric stress tensor I_{2D} and the angle of internal frictionξ

Kinetic model

It has been experimentally proved that the primary products of the reaction between methane and NiO are CO_2 and H_2O despite a relatively small quantity of CO and H_2 which may be considered as the intermediate products existing in the reaction (34-36). The reduction reactions of NiO/Ni with methane in fuel reactor can be described by the following overall reaction equation:

$$CH_4(g) + NiO(s) \rightarrow Ni(s) + 2H_2O(g) + CO_2(g)$$
$$\Delta H_r = 158.35\ kJ/mol \quad (30)$$

In either fuel or air reactor, the reaction rate is affected by various factors such as mass transfer, gas-solid contact and reaction mechanism. Among the variations, chemical reactions involved in air or fuel reactors may be considered as non-catalytic gas-solid reaction and be regarded as the major resistance to the reaction (37). We employed the Shrinking Core Model (SCM) to depict the reaction rate in fuel reactor, which has be successfully utilised in many previous studies (26, 37-39):

$$\frac{dX}{dt} = 3bC^n k_0 \exp(-E_0/RT)(1-X)^{2/3} \quad (31)$$

where C is the bulk concentration of gaseous reactant. The kinetic parameters [27] used in the simulation are listed in Table 1.

Table 1 Kinetic parameters for Ni-based oxygen carrier

	CH_4
k_0($mol^{1-n}m^{3n-2}s^{-1}$)	2.75
E_0 (kJ/mol)	114
n	0.4
b	4

The physical properties and operating parameters adopted in the simulation in the current study are summarised in Table 2.

Table 2 physical properties and operation parameters

Width of Bed (cm)	25
Height of Bed (cm)	60
Temperature (K)	950
Viscosity of Nitrogen (g/cm .s)	$2.3x10^{-4}$
Inlet Fuel Gas Velocity (cm/s)	15
Diameter of Catalyst(μm)	152.5
Density of Particle (g/cm^3)	3.2
Minimum Fluidization Velocity(cm/s)	3.27
Initial Solid Height(cm)	15
Initial Solid Volume Fraction	0.48
Restitution Coefficient(e)	0.8
Wall Restitution Coefficient(e_w)	1.0
Specularity Coefficient (Φ	0.6
Time Interval (s)	10^{-3}-10^{-5}
Grid Size(Dx x Dy) (cm)	0.25x0.25

Geometric model, initial and boundary conditions

The dimensions of the model geometry adopted in the simulation are based on the simulating investigation as reported by Jung and Gamwo (2008) (8). The fuel reactor is 0.15 in diameter and 0.6 m in height. The vessel is assumed to be adiabatic. The grid of fuel reactor employed in the simulation is shown in Figure 2. The appropriate initial and boundary conditions are essential to be defined in the simulation. The Johnson and Jackson slip boundary condition with no frictional contribution for solid phase and granular temperature boundary condition were adopted [37], following the previous study [8].

$$n \cdot \tau_c = -\frac{\sqrt{3\theta}\pi\Phi\rho_S\varepsilon_S g_0 U_{sl}}{6\varepsilon_{S,\max}} \quad (32)$$

$$-n \cdot q = -\frac{\sqrt{3\theta}\pi\Phi\rho_S\varepsilon_S g_0 |U_{sl}|^2}{6\varepsilon_{S,\max}} + \frac{\sqrt{3}\pi\rho_S\varepsilon_S g_0 (1-e_w^2)\theta^{3/2}}{4\varepsilon_{S,\max}} \quad (33)$$

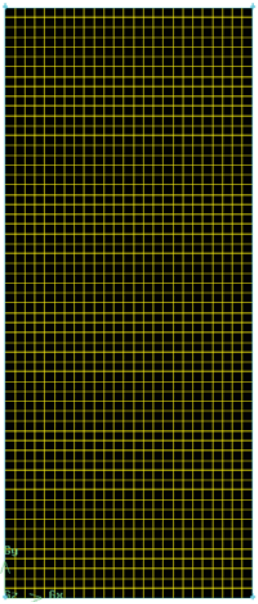

Figure 2. the grid adopted in the simulation of the fuel reactor with the size ratio of 1:4

The simulation was initialised by assuming the fuel reactor to be partly loaded with the oxygen carriers consisting of NiO (60 wt%) supported on $NiMgAl_2O_4$ (40 wt%), where the initial solid volume fraction is 0.48 and the static bed height is 0.15 m. The porosity of the oxygen carrier is 0.36%. Pressure outlet boundary condition at the exit is imposed with the approximation that the reactive flow is well developed. The commercial CFD code ANSYS FLUENT has been adopted in the simulation. The case of heterogeneous reaction was considered. The time step of 0.0001s is chosen for the temporal discretization and 30 iterations per time step are carried out. A convergence criterion of 10^{-3} was selected to specify the maximum residuals between two successive iterations for all concerned parameters. The phase coupled SIMPLE algorithm was employed to describe the pressure-velocity coupling of both gas and solid phases. The second order QUICK scheme is employed to evaluate the convective terms. In the simulation, grid independence test has been undertaken and it was found that the refined mesh with 0.125×0.125 cm has minor impact on the predicted flow behavior and concentrations of both gas and solid phases. Thus, a grid of 0.25×0.25cm has been employed throughout the simulation.

RESULTS AND DISCUSSION

Bubble formation and distributions of reactants and producs in the fuel reactor

To examine the bubble formation, the transient simulations have been performed over a period of 12.75s. The trial simulation has indicated that after this time instant, it seems the flow in the fuel reactor has achieved a sub-steady status. At the beginning of the simulation, the solid oxygen carriers (NiO particles) were assumed to suspend by the inert gas introduced from the bottom of the fuel reactor. The gaseous fuel consisting of 12.5 wt% of methane (CH4) and 87.5 wt% of nitrogen (N2) was fed to the fuel reactor after the simulation reached 5s. Simulation results indicate that the solid particles and gaseous fuel are highly mixed due to the formation of upward gas bubble. Meanwhile, the methane is oxidised by the oxygen within the solid carriers and converted to two main products, H_2O and CO_2.

The instantaneous changes of different parameters and properties of the flow and reaction can be observed from the simulation. Figure 3 shows the distributions of the volume fraction of solid particles, the mass fraction of methane, the mass fraction of H_2O and the mass fraction of CO_2 when the simulation time t = 6.5s. It can be seen that the contour plot of particle volume fraction seems to reasonably capture the important characteristics of the bubbles in the fuel reactor including the formation, rise and burst of bubbles. As the fast rising bubbles would result in a poor mixing between solid particles and gas phase species so that the conversion of methane is reduced significantly, it is essential to monitor and control bubble formation, which will assist the conversion of the fuel gas so as to improve the conversion efficiency. This will be further discussed.

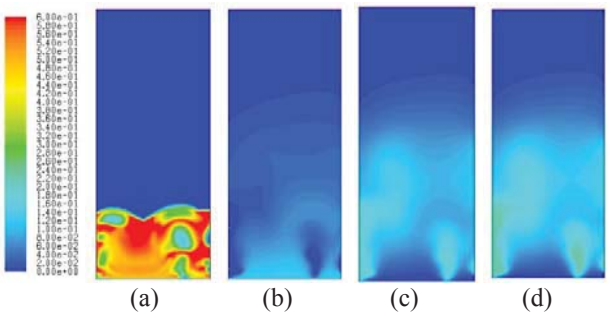

Figure 3. Instantaneous contours of the volume fractions of solid particles and the mass fractions of the reactants and products in the fuel reactor at t = 6.5 s. (a) the volume fraction of solid particles; (b) the mass fraction of methane; c) the mass fraction of H_2O; c) the mass fraction of CO_2.

As mentioned above, the simulation revealed that the flow in the fuel reactor roughly achieved the quasi-steady status at t = 6.5s. It can be seen from Figure 3b that the mass fraction of CH4 decreases linearly along the height of the fuel reactor from the distributor to the outlet while the reverse for the distributions of H2O and CO2 is observed from Figure 3c and 3d. This result is qualitatively consistent with the reality as can be seen from the overall reaction equation (30). Because H2O and CO2 are the reaction products, it is expected that with the consumption of CH4, production of H2O and CO2 in the reduction process should increase. Adanez et al. [33] indicated

that the mass fraction of methane in longitudinal direction predicted by using the shrinking core model decreases linearly along the bed height when referencing from the bottom. Unlike the results obtained by Jung et al.(2008) [8] and Deng et al. (2009)[24] where the bubble phase presented a high concentration of CH4 indicating the bypassing of bubble in the fuel reactor would result in a poor conversion rate due to incomplete combustion, sufficient reaction between methane and solid carriers takes place due to the lower inlet rate of methane. This is consistent with the results obtained from the current simulations. Thus, the bubble fraction contours shown in Figure 3a clearly indicate that the formed bubbles are not 'fast rising bubble' and they may promote the combustion of gaseous fuel CH4. As a result, higher concentrations of products such as H2O and CO2 are founded around bubble phase as can be seen from Figure 3a, c and d.

Redistributions of reactants and products and dynamic parameters variations in fuel reactor

The time evolution of mass fractions of gaseous reactant and products in the dense bed region was captured and recorded, starting at t=5s after the simulation was run, as shown in Figure 4. When t= 8s, the time oscillation of the methane mass fraction seems to enter the quasi-steady status, where the bubble bypassing and the reduction may dictate the involved phenomena observed in the fuel reactor. From Figure 4, it is obvious that the mass fraction of CH_4 oscillates around 0.035. It can be seen from the figure that a rapid increase in the mass fraction of the gaseous products is occurring during the period from t=5 to 8s. This may be attributed to the sufficient reduction. The tendency of the oscillations of CO_2 mass fraction is very similar to that of the methane. The mass fraction of CO_2 sustains a frequent oscillation around 0.16 after 8s, while 0.14 for that of H_2O. These time oscillations indicates that the reduction have reached a quasi-equilibrium after 8s for the fuel reactor adopted in the current study.

Figure 5 shows the variations of the mass fraction of gaseous reactant and products in free board region with the time change. The methane mass fraction in free board region maintains around zero since it has reached quasi-steady state due to the complete combustion of gaseous fuel. A careful observation from Figure 5 indicates that the product mass fractions oscillate around 0.18 for CO_2 and 0.16 for H_2O. Under this condition, the conversion of methane in the fuel reactor can be treated as a nearly complete-combustion. Figure 6 exhibits the mass fraction of Ni. It can be seen from the figure that the Ni mass fraction at the monitor position almost increases linearly with time, a trend typically indicating the reduction to be in quasi-equilibrium status.

Characterizations of bubbling using correlations between velocity fluctuation and volume fraction fluctuation

Bubble formation in dense bed region has a significant impact on the conversion rate of methane in fuel reactor as discussed in the previous section. A cost-effective approach to improve the conversion efficiency is to effectively control bubble formation and bubble sizes. Because the local velocity field is strongly associated with the bubble formation, we propose to introduce the correlation coefficients, aiming to illustrate the correlation between the bubble formation and the flow velocity field. Such correlation may be used to forecast the potential bubble formation and their occurrence so that the gas superficial velocity can be adjusted promptly.

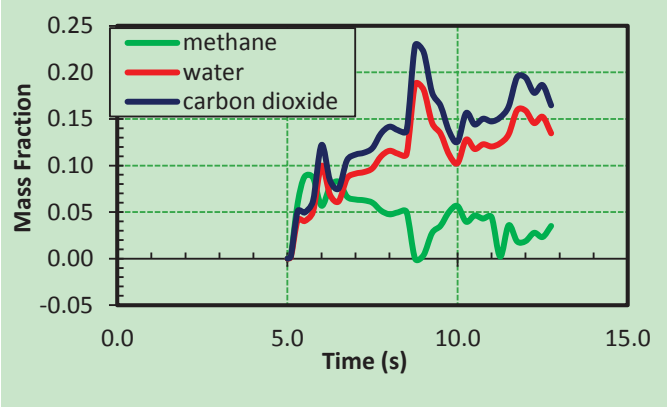

Figure 4. Mass fraction of gaseous reactant and products at x=0.125m, y=0.07m in dense bed region.

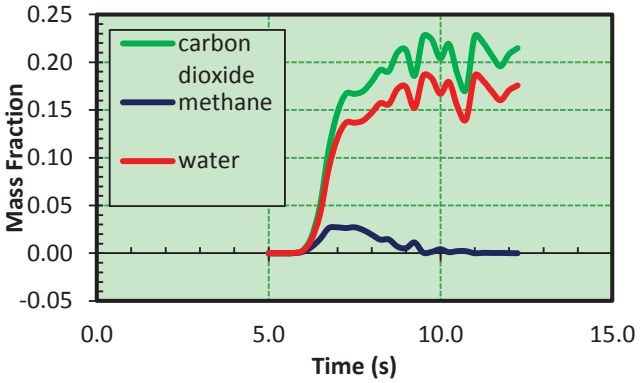

Figure 5. Mass fraction of gaseous reactant and products at x=0.125m, y=0.50m in free board region.

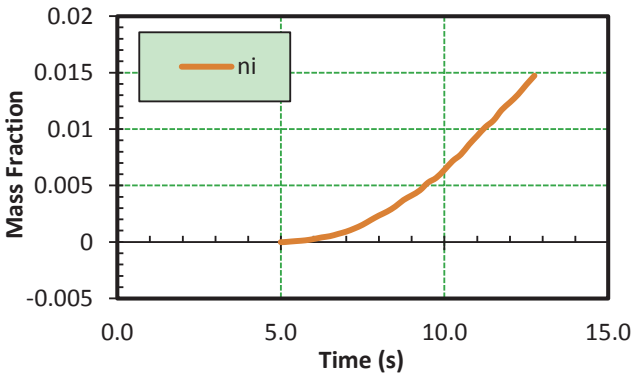

Figure 6. Mass fraction of N_i at x=0.125m, y=0.07m in dense bed region.

$$R_{\varepsilon'\varepsilon'}(\Delta h)=\frac{\overline{\varepsilon_s'(h_0)\varepsilon_s'(h_0+\Delta h)}}{\overline{\varepsilon_s'^2(h_0)}} \quad (34)$$

$$R_{\varepsilon'u_s'}(\Delta h)=\frac{\overline{\varepsilon_s'(h_0)u_s'(h_0+\Delta h)}}{\sqrt{\overline{\varepsilon_s'^2(h_0)}}\sqrt{\overline{u_s'^2(h_0)}}} \quad (35)$$

$$R(t)=\frac{\overline{\varepsilon_s'(t,r_0,h_0)\phi_g'(t+\tau,r_0,h_0)}}{\sqrt{\overline{\varepsilon_s'^2(t,r_0,h_0)}}\sqrt{\overline{\phi_g'^2(t,r_0,h_0)}}} \quad (36)$$

where, $R(\Delta h)$ and $R(t)$ are the spatial correlation coefficient and time correlation coefficient, respectively; ϕ_g' and ε_s' are the local fluid dynamic parameter fluctuation and volume fraction fluctuation at the given spatial position and given time.

Figure7a shows the spatial correlation coefficient R(Δh) relating with the local solid volume fraction evolution. Figure7b depicts the spatial correlation coefficient which indicates the correlation between the solid volume fraction and particle vertical velocity components u_s. It can be seen from Figure7 that two bubbles exist around the heights in the ranges of y=0.05-0.07m and 0.11-0.14m in the dense bed region while a bubble bursting takes place at above 0.14m vertically. The correlations to indicate bubble formation as shown in Figure7 are quantitatively consistent with Figure 3a as expected. Figure 8 shows the time correlation of $\overline{\varepsilon_s'u_s'}$, calculated based on the period from 5.0 to 12.75s. It seems that a rapid reduction on the value of the correlation curve implies that a bubble occurrence, which roughly covers the period of 6.75 to 8s, 9.1 to 9.5s, 10.7 to 11s and 11.6 to 11.8s, respectively.

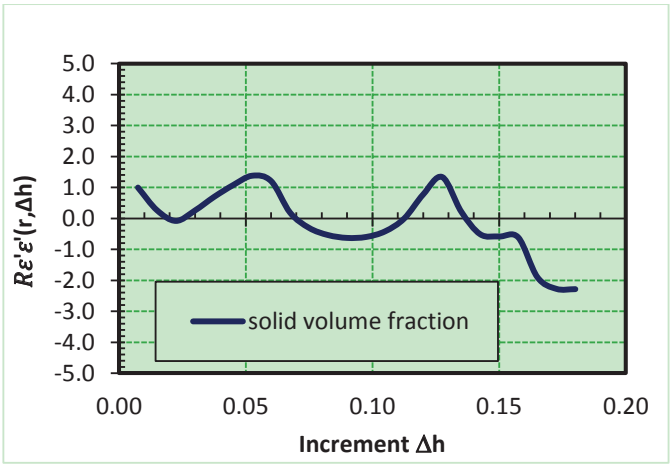

(a)

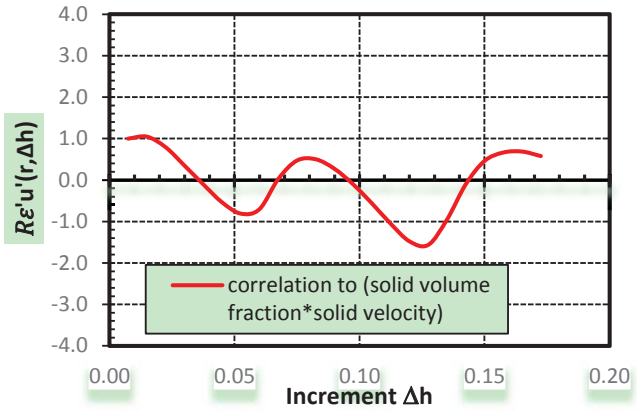

(b)

Figure7. Spatial correlation coefficient to identify the bubble formation at x=0.17m, y=0-0.18m a) correlations of $\varepsilon_s u_g$ and $\varepsilon_s P_g$ separately; b) correlation of $\overline{\varepsilon_s'u_s'}$ at 6.5s.

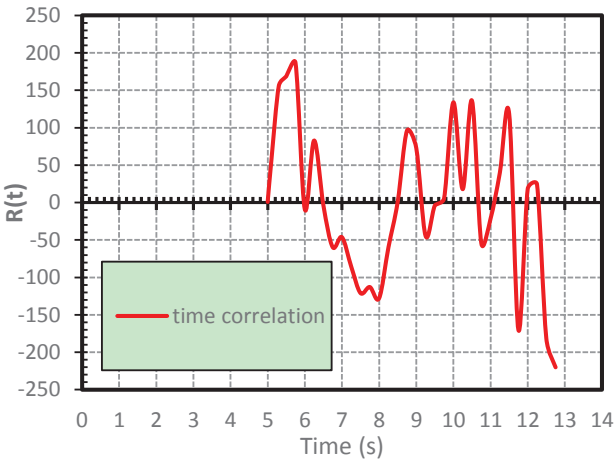

Figure 8. Time correlation relating the bubble formation with $\overline{\varepsilon_s'u_s'}$ at x=0.125m, y=0.07.

CONCLUSION

A 2-D numerical model describing the hydrodynamics and the reaction kinetics of CLC process in fuel reactor has been developed by coupling the heterogeneous reaction to the gas-solid flow with NiO as the oxygen carrier and methane as the gaseous fuel. The transient behaviours of various properties related to the CLC including the velocity and volume fraction profiles, formed bubble and the species distributions were investigated using the developed CFD modelling. The main conclusions drawn from the current study are:

1) The evolution of bubble formation in the fuel reactor was traced and the bubble motions which were responsible for the sufficient mixing of the oxygen carrier and gaseous fuel were observed from the simulation. It was revealed that methane is almost completely combusted owing to the use of lower inlet velocity for gaseous fuel, which may assist a sufficient mixing between the solid carriers and methane.

2) A parameter to indicate the bubble formation by correlating the local volume fractions with dynamic parameters of reactive flow was proposed as an indicator of the occurrence of the time-dependent bubble in the reactor. This parameter has a potential to be applied to the CLC for controlling the bubbling phenomenon because the occurrence of the bubbles at specific positions is highly correlated with the local large eddies embedded in the flow.

ACKNOWLEDGEMENT

This work was carried out at the International Doctoral Innovation Centre (IDIC). The authors acknowledge the financial support from Ningbo Education Bureau, Ningbo Science and Technology Bureau, China's MoST and The University of Nottingham. The work is also partially supported by EPSRC (Grant no. EP/G037345/1).

REFERENCES

1. Lyngfelt A, Leckner B. Technologies for CO2 separation. Minisymposium on CO2 capture and storage [Internet]. 1999 15/05/2014:[22-35 pp.]. Available from: http://www.entek.chalmers.se/~anly/co2/co2.htm.
2. Lyngfelt A, Leckner B, Mattisson T. A fluidized-bed combustion process with inherent CO2 separation; application of chemical-looping combustion. Chemical Engineering Science. 2001;56:3101–13.
3. Rüdisüli M, Schildhauer TJ, Biollaz SMA, van Ommen JR. Scale-up of bubbling fluidized bed reactors — A review. Powder Technology. 2012;217:21-38.
4. Noorman S, Annaland MV, Kuipers JAM. Experimental validation of packed bed chemical-looping combustion. Chemical EngineeringScience. 2010;65:92--7.
5. Fan L, Li F, Ramkumar S. Utilization of chemical looping strategy in coal gasification processes. Particuology. 2008;6:131–42.
6. Gnanapragasam NV, Reddy BV, Rosen MA. Hydrogen production from coal using coal direct chemical looping and syngas chemical looping combustion systems:assessment of system operation and resource requirements. International Journal of Hydrogen Energy. 2009;34:2606–15.
7. Son SR, Kim SD. Chemical-looping combustion with NiO and Fe2O3 in a thermobalance and circulating fluidized bed reactor with double loops. Industrial Engineering and Chemical Research. 2006;45(8):2689–96.
8. Jung J, Gamwo IK. Multiphase CFD-based models for chemical looping combustion process: Fuel reactor modeling. Powder Technology. 2008;183(3):401-9.
9. Johansson M, Mattisson M, Rydén M, Lyngfelt A. Carbon Capture via Chemical-Looping Combustion and Reforming. International Seminar on Carbon Sequenstration and Climate Change; October 24–27 Rio de Janeiro,Brazil2006.
10. Adanez J, Abad A, Garcia-Labiano F, Gayan P, de Diego LF. Progress in Chemical-Looping Combustion and Reforming technologies. Progress in Energy and Combustion Science. 2012;38(2):215-82.
11. Hossain MM, de Lasa HI. Chemical-looping combustion (CLC) for inherent separations—a review. Chemical Engineering Science. 2008;63(18):4433-51.
12. Kolbitsch P, Bolhàr-Nordenkampf J, Pröll T, Hofbauer H. Operating experience with chemical looping combustion in a 120kW dual circulating fluidized bed (DCFB) unit. International Journal of Greenhouse Gas Control. 2010;4(2):180-5.
13. de Diego LF, García-Labiano F, Gayán P, Celaya J, Palacios JM, Adánez J. Operation of a 10 kWth Chemical-Looping Combustor. Fuel. 2007;86:1036-45.
14. Johansson E, Mattisson T, Lyngfelt A, Thunman H. Combustion of Syngas and Natural Gas in a 300 W Chemical-Looping Combustor. Chemical Engineering Research and Design. 2006;84(9):819-27.
15. Kolbitsch P, Bolhàr-Nordenkampf J, Pröll T, Hofbauer H. Comparison of two Ni-based oxygen carriers for chemical looping combustion of natural gas in 140kW continuous looping operation. Ind Eng Chem Res. 2009;48:5542-7.
16. Forero CR, Gayán P, de Diego LF, Abad A, García-Labiano F, Adánez J. Syngas combustion in a

500 Wth Chemical-Looping Combustion system using an impregnated Cu-based oxygen carrier. Fuel Processing Technology. 2009;90(12):1471-9.
17. Mattisson T, Johansson M, Lyngfelt A. The use of NiO as an oxygen carrier in chemical-looping combustion. Fuel. 2006;85(5-6):736-47.
18. Dueso C, García-Labiano F, Adánez J, de Diego LF, Gayán P, Abad A. Syngas combustion in a chemical-looping combustion system using an impregnated Ni-based oxygen carrier. Fuel. 2009;88(12):2357-64.
19. Linderholm C, Mattisson T, Lyngfelt A. Long-term integrity testing of spray-dried particles in a 10-kW chemical-looping combustor using natural gas as fuel. Fuel. 2009;88(11):2083-96.
20. Garcı F, de Diego LF, Gaya P, Dueso C. Effect of Fuel Gas Composition in Chemical-Looping Combustion with Ni-Based Oxygen Carriers. 1. Fate of Sulfur. Ind Eng Chem Res. 2009;48:2499–508.
21. Shuai W, Guodong L, Huilin L, Juhui C, Yurong H, Jiaxing W. Fluid dynamic simulation in a chemical looping combustion with two interconnected fluidized beds. Fuel Processing Technology. 2011;92(3):385-93.
22. Seo MW, Nguyen TDB, Lim YI, Kim SD, Park S, Song BH, et al. Solid circulation and loop-seal characteristics of a dual circulating fluidized bed: Experiments and CFD simulation. Chemical Engineering Journal. 2011;168(2):803-11.
23. Mahalatkar K, Kuhlman J, Huckaby ED, O'Brien T. Computational fluid dynamic simulations of chemical looping fuel reactors utilizing gaseous fuels. Chemical Engineering Science. 2011;66(3):469-79.
24. Deng Z, Xiao R, Jin B, Song Q. Numerical simulation of chemical looping combustion process with CaSO4 oxygen carrier. International Journal of Greenhouse Gas Control. 2009;3(4):368-75.
25. Kruggel-Emden H, Rickelt S, Stepanek F, Munjiza A. Development and testing of an interconnected multiphase CFD-model for chemical looping combustion. Chemical Engineering Science. 2010;65(16):4732-45.
26. Wang S, Lu H, Zhao F, Liu G. CFD studies of dual circulating fluidized bed reactors for chemical looping combustion processes. Chemical Engineering Journal. 2014;236:121-30.
27. Zafar Q, Abad A, Mattisson T, Gevert B. Reaction kinetics of freeze-granulatedxygen carrier particles for chemical-looping combustion. Energy & Fuels. 2007;21:610-8.
28. Gunn DJ. Transfer of heat or mass to particles in fixed and fluidised beds. International Journal of Heat and Mass Transfer. 1978;21(4):467-76.
29. Wang Y, Zou Z, Li H, Zhu Q. A new drag model for TFM simulation of gas–solid bubbling fluidized beds with Geldart-B particles. Particuology. 2013;In Press, Corrected Proof:DOI: 10.1016/j.partic.2013.07.003.
30. Sundaresan S. Modeling the hydrodynamics of multiphase flow reactors Current status and challenges. AIChE Journal. 2000;46:1102-5.
31. Ding JG, D. A Bubbling Fluidization Model Using Kinetic theory of granular flow. AIChE Journal. 1990;36(4).
32. Patil DJ, van Sint Annaland M, Kuipers JAM. Critical comparison of hydrodynamic models for gas–solid fluidized beds—Part I : bubbling gas–solid fluidized beds operated with a jet. Chemical Engineering Science. 2005;60(1):57-72.
33. LUN CKK, SAVAGE SB, JEFFREY DJ, CHEPURNIY N. kinetic theories for granular flow-inelastic particles in Couette-flow and slightly inelastic particles in a general flow field. J Fluid Mech. 1984;140:223-56.
34. Iliuta I, Tahoces R, Patience GS, Rifflart S, Luck F. Chemical-looping combustion process: Kinetics and mathematical modeling. AIChE Journal. 2010;56(4):1063-79.
35. Abad A, Adánez J, García-Labiano F, De Diego LF, Gayán P, Kolbitsch P, et al. CLC Modeling the fuel-reactor at fast fluidization–Conversion of CH4 using a NiO-based oxygen carrier in a 120kWth unit. Les Rencontres Scientifiques de l'IFP-1st International Conference on Chemical Looping; 17-19 March; Lyon, Francia 2010.
36. Dewaele O, Froment GF. TAP Study of the Mechanism and Kinetics of the Adsorption and Combustion of Methane on Ni/Al2O3 and NiO/Al2O3. Journal of Catalysis. 1999;184:499–513.
37. Zafar Q, Abad A, Mattisson T, Gevert B, Strand M. Reduction and oxidation kinetics of Mn3O4/Mg–ZrO2 oxygen carrier particles for

chemical-looping combustion. Chemical Engineering Science. 2007;62(23):6556-67.
38. JOHNSON PC, JACKSON R. Frictional-collisional constitutive relation for granular materials with application to plane shearing. J Fluid Mech. 1987;176:67-93.
39. Abad A, Adánez J, García-Labiano F, de Diego LF, Gayán P, Celaya J. Mapping of the range of operational conditions for Cu-, Fe-, and Ni-based oxygen carriers in chemical-looping combustion. Chemical Engineering Science. 2007;62(1-2):533-49.